Water Research X 24 (2024) 100239

Contents lists available at ScienceDirect

Water Research X

journal homepage: www.sciencedirect.com/journal/water-research-x

Perfluoroalkyl functionalized-Au nanoparticle sensor: Employing rate of spectrum shifting for highly selective and sensitive detection of per- and polyfluoroalkyl substances (PFASs) in aqueous environments

Jihyeun Jung [a], Junyoung Park [a,b], Jong Kwon Choe [a,b], Yongju Choi [a,b,*]

[a] Department of Civil & Environmental Engineering, Seoul National University, 1 Gwanak-ro, Gwanak-gu, Seoul 08826, Republic of Korea
[b] Institute of Construction and Environmental Engineering, Seoul National University, 1 Gwanak-ro, Gwanak-gu, Seoul 08826, Republic of Korea

ARTICLE INFO

Keywords:
PFASs
Sensor
Fluorous interaction
Gold nanoparticle
Colorimetric sensor

ABSTRACT

Per- and polyfluoroalkyl substances (PFASs) are emerging contaminants detected ubiquitously and have negative impacts on human health and ecosystem; thus, developing *in-situ* sensing technique is important to ensure safety. Herein, we report a novel colorimetric-based sensor with perfluoroalkyl receptor attached to citrate coated gold nanoparticles (Citrate-Au NPs) that can detect several PFASs including perfluorocarboxylates with different chain lengths (PFHxA, PFOA, PFNA, PFDA), perfluorooctanoic sulfonate (PFOS), and perfluorooctanoic phosphonate (PFOPA). The sensor detects PFASs utilizing fluorous interaction between PFASs and the perfluoroalkyl receptor of Citrate-Au NPs in a solution at a fixed salt concentration, inducing changes in nanoparticle dispersity and the solution color. The rate of spectrum shift was linearly dependent on PFASs concentrations. Citrate-Au NPs with size between 29 – 109 nm were synthesized by adjusting citrate/Au molar ratios, and 78 nm showed the best sensitivity to PFOA concentration (with level of detection of 4.96 μM). Citrate-Au NPs only interacted with PFASs with perfluoroalkyl length > 4 and not with non-fluorinated alkyl compound (nonanoic acid). The performance of Citrate-Au NP based sensor was strongly dependent on the chain length of the perfluoroalkyl group and the head functional group; higher sensitivity was observed with longer chain over shorter chain, and with sulfonate functional group over carboxylate and phosphonate. The sensor was tested using real water samples (i.e., tap water, filtered river water), and it was found that the sensor is capable of detecting PFASs in these conditions if calibrated with the corresponding water matrix. While further optimization is needed, this study demonstrated new capability of Citrate-Au NPs based sensor for detection of PFASs in water.

1. Introduction

Per-and polyfluoroalkyl substances (PFASs) are a group of compounds that have recently received the most attention. Widespread applications of PFASs in industrial products, combined with their persistence, result in ubiquitous presence of PFASs in the aquatic environment to cause potential risks to humans and other organisms (Garnett et al., 2021; Pétré et al., 2021). Exposure to PFASs-containing water has been found to pose acute and chronic harms to living organisms through bioaccumulation and in-vivo biotransformation (Fenton et al., 2021; Harris et al., 2017; Zheng et al., 2021). Because of the current threat of PFASs water contamination by PFASs, it is urgently needed to develop a sensor that enables easy and timely detection of PFASs in water.

Colorimetric method is a promising sensing technique to monitor on-site detection of water contaminants. Colorimetric sensors have advantages in easy-handling and rapid signal gain, and often can be incorporated into hand-held devices (Ryu et al., 2021; Umapathi et al., 2022). Previous studies have developed sensing techniques employing color development or color change caused by ion paring between PFASs and a cationic dye (Amin et al., 2020; Menger et al., 2022), by deactivation of a nano-sized catalyst that oxidizes 3,3′,5,5′-tetramethylbenzidine in the presence of PFASs (Guo et al., 2023; Liu et al., 2019), and by adsorption of PFASs to a perfluoroalkylated dye (Taylor et al., 2023, 2021). Although these studies showed promise, none of the colorimetric sensing platforms described therein have been fully demonstrated to be widely

* Corresponding author at: Department of Civil & Environmental Engineering, Seoul National University, 1 Gwanak-ro, Gwanak-gu, Seoul 08826, Republic of Korea
E-mail address: ychoi@snu.ac.kr (Y. Choi).

https://doi.org/10.1016/j.wroa.2024.100239
Received 30 May 2024; Received in revised form 15 July 2024; Accepted 17 July 2024
Available online 28 July 2024

applicable in various water media with sufficient selectivity and sensitivity to PFASs (Menger et al., 2021; Wang et al., 2021). Therefore, continued efforts are necessary for developing colorimetric sensing platforms that selectively and sensitively detect of PFASs in water.

Herein, we developed a colorimetric sensing strategy that utilizes spectrum shifting characteristics of a solution containing gold nanoparticles (Au NPs) functionalized with citrate (henceforth denoted as Citrate-Au NPs) to detect PFASs in water via a perfluoroalkyl receptor. Au NPs are frequently employed to design an optical sensing platform for their high efficiency in absorbing and scattering light (Chen et al., 2018; Piella et al., 2016). In addition, Au NPs are easily synthesized and are easy to modify to alter surface characteristics or add receptors that bind to target molecules (Aldewachi et al., 2018; Fang et al., 2017; Lee et al., 2021). Perfluoroalkyl receptors are expected to endow high selectivity to PFASs by fluorous interaction, a phenomenon that the perfluoroalkyl chain of a PFAS binds to a perfluoroalkyl surface (Johnson et al., 2019; Osei-Prempeh et al., 2008). A colorimetric sensing strategy utilizing spectrum shifting of negatively-charged Au NPs via their destabilization in response to electrolyte addition has often been executed in biosensor developments (Bigdeli et al., 2017; Lee et al., 2008), while, to our knowledge, it has not been used to develop PFASs sensors. The general working principle of the spectrum shifting assay using Citrate-Au NPs is as follows. Citrate-Au NPs in pure water are electrostatically stabilized due to the negative charge induced by citrate anions on their surface. In the absence of target chemicals, Citrate-Au NPs lose their stability by salt addition, leading to shifting of the absorbance spectrum of the solution. When target chemicals are present, they interfere with the particle destabilization process by attaching to receptors on the surface, thereby altering the spectrum shifting characteristics (Fig. 1).

Our colorimetric sensing strategy has been developed by i) synthesizing Citrate-Au NPs under different conditions to yield NPs with various size ranges, ii) investigating the changes in light absorbance spectra over time after adding PFASs and salt to the NPs, and iii) extracting the quantity that aligns well with the amount of PFAS added, and iv) identifying a size range that fits best for PFASs detection. The sensing strategy was investigated for selectivity by testing PFASs with various chain lengths and functional groups, and compounds exhibiting structural similarity to PFASs. To investigate the practical applicability of the sensing strategy, it was tested in real water samples and synthetic water samples containing major water constituents.

2. Results and discussion

2.1. Characterization and stability of citrate-Au NPs

Variation of the citrate/Au ratio enabled controlling the size of Citrate-Au NPs. Citrate/Au ratio of 0.5, 0.8, 1, and 5 mmol/mmol yielded the Au NPs with volume-weighted mean sizes of 109, 78, 49, and 29 nm (Figs. 2A and S1), respectively, as determined by the dynamic light scattering (DLS) analysis. The DLS-determined mean size was monodistributed for all cases and coincided well with the size observed in transmission electron microscopy (TEM) images (Fig. S2). The decrease in mean size with increasing citrate/Au ratio is attributed to the dual role of citrate as a reducing agent and surface coating material during Au NPs synthesis. Previous studies demonstrated that, at higher citrate/Au ratio, the Au particle nucleus is generated rapidly and then is soon coated with citrate, which prevents further particle size growth (Polte et al., 2010; Zabetakis et al., 2012).

The Citrate-Au NPs had a ζ potential range from −23 mV to −43 mV with smaller-sized NPs (i.e., those synthesized at higher citrate/Au ratio) showing more negative ζ potential (Fig. 2B). This difference is mainly attributed to the different degree of citrate deprotonation at different citrate/Au ratios (Ji et al., 2007; Ojea-Jiménez et al., 2010). Because sodium citrate, a base, was added to an acid (i.e., $HAuCl_4$) solution when synthesizing Citrate-Au NPs, the solution pH decreased as higher citrate/Au ratio was employed. The pH of the Au NPs solution was 6.2 for 29-nm NPs (citrate/Au ratio = 5 mmol/mmol) and 3.2 for 109-nm NPs (citrate/Au ratio = 0.5 mmol/mmol) (Fig. 2B). The pK_a values of citrate (pK_{a1} = 3.15, pK_{a2} = 4.78, and pK_{a3} = 6.40 (Lambros et al., 2022)) indicate substantial changes in citrate deprotonation within a pH range from 3.2 to 6.2.

The Citrate-Au NPs yield fraction data (Fig. 2C), defined as the ratio of the Au NPs in solution ($M_{Au\ NPs}$) relative to the total amount of added $HAuCl_4$ (M_{Au0}), showed that the Au NPs with mean size equal to or smaller than 78 nm were more stable than the ones with 109 nm in mean size. Au NPs with 29, 49, and 78 nm in size exhibited yield fractions greater than 0.90 with standard deviations of ≤0.04. On the other hand, the yield fraction of 109-nm-sized Au NPs was 0.80, indicating that only 80% of the synthesized NPs remained suspended in solution with the rest

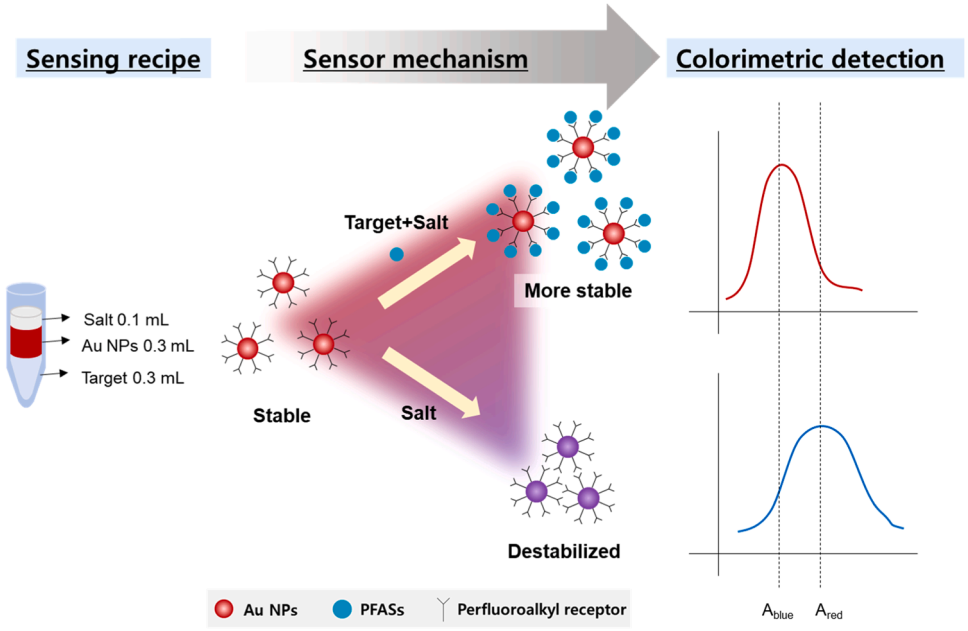

Fig. 1. Schematic of the colorimetric sensing strategy investigated in the current work.

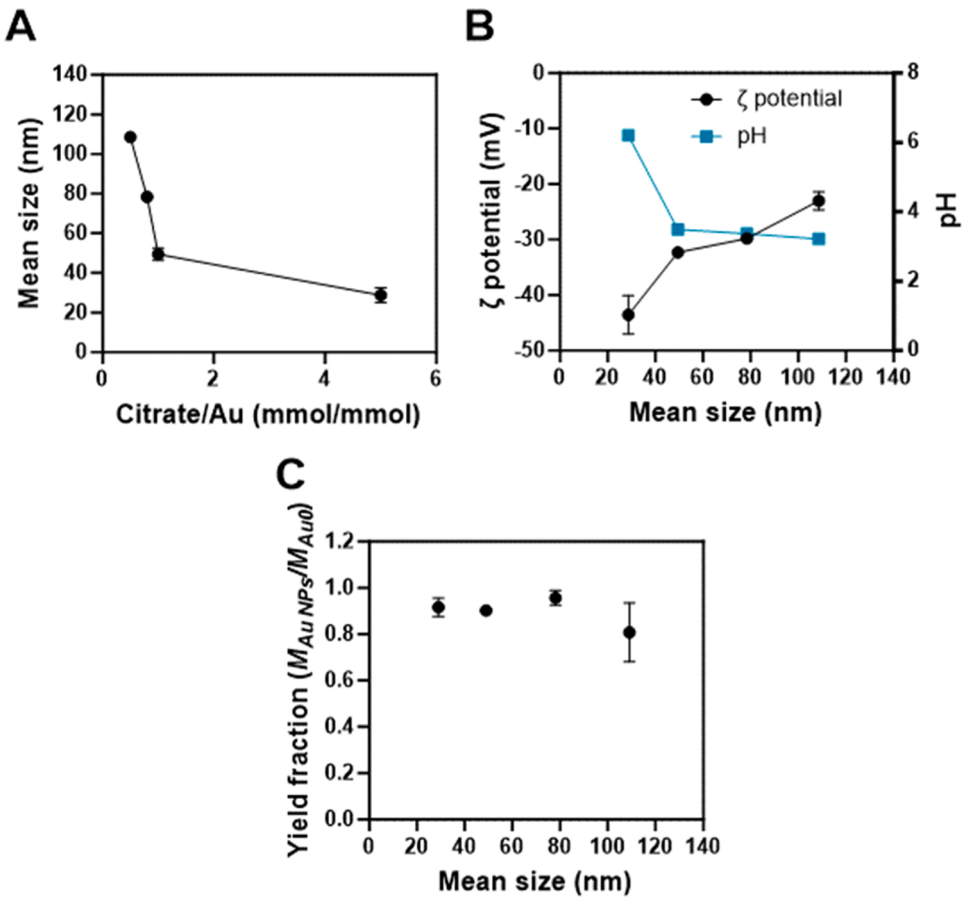

Fig. 2. (A) Hydrodynamic mean size of Citrate-Au NPs with variation of citrate/Au ratio, (B) ζ potential of Citrate-Au NPs and pH of the solution with variation of particle mean size, and (C) yield fraction of Citrate-Au NPs ($M_{Au\ NPs}/M_{Au0}$) with variation of particle mean size.

being removed by aggregation and precipitation. Relatively large standard deviation (0.13) was also observed for the yield fraction of 109-nm-sized Au NPs, undermining the reproducibility of their synthesis. Because of these drawbacks, 109-nm-sized Au NPs were excluded from further evaluation. The relative instability of the 109-nm-sized Au NPs is attributed to their larger size and less negative ζ potential (Fig. 2B), both of which reduce the stability of NPs (Kobayashi et al., 2005; Pochapski et al., 2021).

2.2. Response of citrate-Au NPs sensor to perfluorooctanoate (PFOA)

The colorimetric assay developed herein is conducted by combining a NaCl solution with a water sample and Citrate-Au NPs solution to produce a solution high in electrolytes (0.043 M NaCl), which is then immediately submitted for UV–Vis spectrometry analysis. The electrolyte addition compresses the electrical double layer of the Citrate-Au NPs, resulting in aggregation of the NPs (Barisik et al., 2014; Wei et al., 2022). The aggregate formation by this mechanism is expressed as blue shift in color and change in the absorbance ratio of the blue and the red spectrum peak (i.e., A_{blue}/A_{red}) via UV/Vis spectrometry. A perfluoralkyl receptor that contains six perfluoroalkyl carbons with a spacer of two fully hydrogenated alkyl carbons is grafted to the surface of Au NPs via an Au-S bond. Binding of PFASs molecules to the receptor alters the destabilization characteristics of negatively-charged Citrate-Au NPs in response to NaCl addition. By recording the A_{blue}/A_{red} values, the relative difference in the destabilization characteristics is identified for solutions with different PFAS concentrations.

Experiments verified that the PFAS sensing mechanism described above indeed worked. When a blank solution, a Citrate-Au NP solution, and the NaCl solution were combined, A_{blue}/A_{red} decreased over time, indicating a blue shift in color (Figs. S3 and S4). Precipitation of some larger-sized aggregates also occurred, as could be identified visually and by a decrease in absolute absorbance values at the end of the measurements. On the other hand, when 78-nm Citrate-Au NPs were combined with a highly-concentrated PFOA solution (107.14 or 214.29 μM) and the NaCl solution, A_{blue}/A_{red} stayed constant over time, indicating that the presence of excessive amounts of PFOA prevented the blue shift (i.e., fully stabilized the Au NPs). TEM images of Citrate-Au NPs combined with a 107.14 μM PFOA solution and the NaCl solution provided a clear evidence that the Citrate-Au NPs remained dispersed. In contrast, when a blank solution was used, Citrate-Au NPs aggregated into larger-sized clusters upon the addition of NaCl (Fig. S5). The likely mechanism for this PFOA-induced stabilization of Citrate-Au NPs is as follows. When PFOA is attached to the perfluoroalkyl receptor of Citrate-Au NPs, the anionic functional group of PFOA, carboxylate, is directed toward the aqueous solution (Fig. S6). Because of the longer chain length (eight carbons) of PFOA than citrate (two carbons), PFOA extends the distance from the Au NPs' surface that exhibits negative electric potential. Therefore, the Au NPs become less sensitive to the electrical double layer compression via electrolyte addition.

Except for the two fully-stabilized cases, the rate of change in A_{blue}/A_{red} decreased as PFOA concentration increased, approaching the endpoint of A_{blue}/A_{red} for blank target solutions. In other words, in most cases, PFOA retarded the aggregation of Au NPs. Thus, it was the rate of blue shift that could effectively determine the PFOA concentration using Citrate-Au NPs. Assuming that the change of the blue shift follows an exponential function with a starting point of $(A_{blue}/A_{red})_{stable}$ (i.e., A_{blue}/A_{red} when the NPs are fully stable) to an endpoint of $(A_{blue}/A_{red})_{end}$, it was represented by the following equation:

$$(A_{blue}/A_{red})_t = (A_{blue}/A_{red})_{end} + \left[(A_{blue}/A_{red})_{stable} - (A_{blue}/A_{red})_{end}\right] \times e^{[-k\times(t+B)]}. \quad (1)$$

where $(A_{blue}/A_{red})_t$ is the absorbance ratio at time t, k is the rate constant of spectrum shift (sec^{-1}), and B (>0) is the fitting parameter (sec). $(A_{blue}/A_{red})_{stable}$ was determined as the A_{blue}/A_{red} at the beginning of absorbance measurement run at the highest PFOA concentration and $(A_{blue}/A_{red})_{end}$ as the A_{blue}/A_{red} at the end of absorbance measurement run using a blank sample. Eq. (1) fitted very well with the experimental data for PFOA concentration range of 0 – 26.79 μM (for 49- and 78-nm mean size) or 0 – 53.57 μM (for 29-nm mean size), with coefficient of determination (R^2) greater than 0.91.

2.3. Sensor performance of citrate-Au NPs

It was verified that the rate constant of spectrum shift, k, could be used to determine PFOA concentration in an aqueous solution. The rate constant was negatively correlated with PFOA concentration at a range of 0 – 26.79 μM (for 49- and 78-nm mean size) or 0 – 53.57 μM (for 29-nm mean size) (Fig. 3). The correlation was fairly linear with R^2 of 0.87 – 0.99. This study is the first application of spectrum shift rate to determine chemical concentration using citrate-reduced Au NPs. Previous studies used spectrum shift itself but not the rate of the shift. Because the time-dependence of the spectrum shift was not reported in the previous studies, we could not identify the essential role of target chemicals on the aggregation of citrate-reduced Au NPs in these studies. Future studies should explore the aggregation mechanism of citrate-reduced Au NPs for a wider range of target chemicals.

Among the Citrate-Au NPs tested, the largest NPs yielded the highest sensitivity toward PFOA. The slope of the linear calibration curve for 78-nm-sized Au NPs (-1.03×10^{-3} */sec*/μM) was 2000-fold steeper than that of 29-nm-sized Au NPs (-5.3×10^{-5} */sec*/μM). The higher sensitivity toward PFOA for the larger-sized NPs is mainly attributed to their smaller surface area. Because surface area is inversely proportional to the diameter of spherical particles at a fixed total particle mass, larger-sized Citrate-Au NPs require less amount of PFOA to alter their surface chemistry. The slope of the linear regression curves shows that a relatively small change in the size may result in dramatic difference in the sensitivity of sensing.

2.4. Sensor response to different molecular structures of targets

Testing the response of the 78-nm-sized Citrate-Au NPs sensor to various molecules revealed that the sensor was highly specific toward molecules containing perfluoroalkyl groups compared to others. The sensor responded sensitively perfluorononanoate (PFNA) over a μM

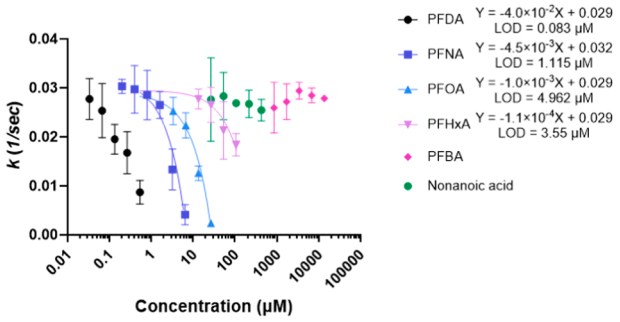

Fig. 4. Response of Citrate-Au NPs sensor to various target compounds: perfluoroalkyl carboxylates with different chain lengths (i.e., PFDA, PFNA, PFOA, PFHxA, and PFBA) and nonanoic acid.

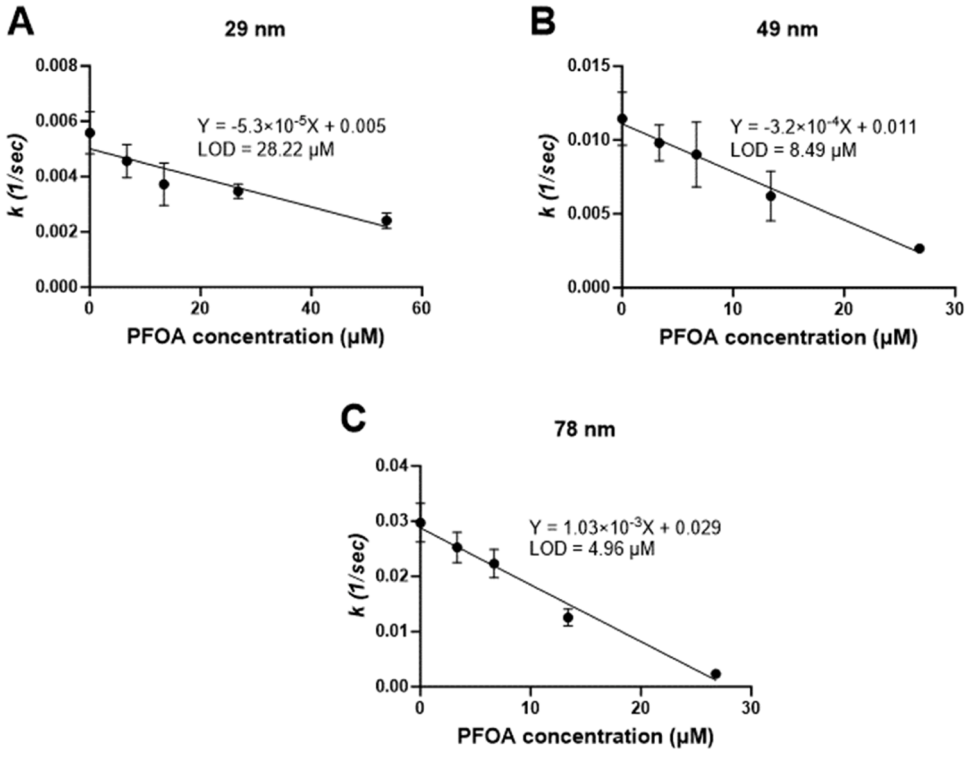

Fig. 3. PFOA calibration curves constructed using Citrate-Au NPs with different mean sizes: (A) 29 nm, (B) 49 nm, and (C) 78 nm.

range while it did not show any response to nonanoic acid (i.e., a no-fluorine-containing counterpart of PFNA) even at a sub-mM level (Fig. 4). This result represents high specificity of intermolecular C-F…F-C interaction (i.e., fluorous interaction) compared to C-F…H-C interaction. Previous studies demonstrated that fluorine in a perfluoroalkylated molecule directly interacts with fluorine in an adjacent perfluoroalkylated molecule (Robalo et al., 2021; Omorodion et al., 2015). In contrast, C-F…H-C interaction is not favorable due to the surface and cohesive energy difference between perfluoroalkyl groups and fully hydrogenated alkyl groups (Dalvi and Rossky, 2010; Jiang et al., 2021; Krafft and Riess, 2009), as well as the high rotation energy of fully hydrogenated alkyl chains (Ellis et al., 2004; Jing et al., 2009).

The sensor response to perfluoroalkyl carboxylates (PFCAs) with different number of perfluorinated carbons demonstrated that the chain length played an important role in the sensitivity of the 78-nm-sized Citrate-Au NPs sensor. Fig. 4 displays the sensor response to PFCAs with different number of perfluorinated carbons [3, 5, 7, 8, and 9 for perfluorobutanoate (PFBA), perfluorohexanoate (PFHxA), PFOA, PFNA, and perfluorodecanoate (PFDA), respectively]. As the number of perfluorinated carbons increased from 5 (PFHxA) to 9 (PFDA), the slope of the calibration curve increased 330-fold (i.e., from -1.2×10^{-4} */sec/*μM to -4.0×10^{-2} */sec/*μM). However, the sensor did not respond to PFBA at all although PFBA was tested up to higher concentration (13 mM) than the others. Studies have suggested that fluorous interaction requires perfluoroalkyl chains longer than a certain length (Du et al., 2016; Pollice and Chen, 2019; Santiago et al., 2023) and the terminal functional groups can disturb the interaction (Kiss et al., 2001). Three perfluorinated carbons that PFBA possesses may be insufficient to attract the perfluoroalkyl receptor with six perfluorinated carbons via fluorous interaction. Electrostatic repulsion between carboxylic groups in PFBA and Citrate-Au NPs, which hinders PFBA from approaching the receptor is another plausible description for the experimental result.

Analysis of the percent of perfluorooctane phosphonate (PFOPA), PFNA, and perfluorooctane sulfonate (PFOS) bound to Citrate-Au NPs relative to the initially added amount confirmed that the PFASs–receptor binding occurs as long as the PFASs possess perfluoroalkyl chains longer than a certain length. For PFOPA, PFNA, and PFOS, all of which have a perfluoroalkyl carbon chain length of eight, 52.3%, 75.5%, and 86.1%, respectively, attached to Citrate-Au NPs relative to the initially added amount (Fig. 5B). The order of the affinity of the three PFASs to Citrate-Au NPs aligned well with the order of sensor sensitivity. The slopes of linear calibration curve were -2.6×10^{-3} /sec/μM for PFOPA, -4.5×10^{-3} /sec/μM for PFNA, and -1.1×10^{-2} /sec/μM for PFOS (Fig. 5A). The influence of functional groups in PFASs on fluorous interaction in an aqueous solution has not been identified as much clearly as that of perfluroalkyl chain length. The net negativity of PFOPA, PFNA, and PFOS were calculated with density functional theory (DFT) simulation as −1.449, −0.800, and −0.663, which was in inverse order of their binding affinity to Citrate- Au NPs (Fig. 5C). As PFASs with lower net negativity tends to have weaker hydrogen bonding with water molecules, they may bind more favorably to a perfluoroalkyl receptor. In addition, because both the surface of Citrate-Au NPs and functional groups in PFAS are negatively charged, the electrostatic repulsion between the two should be weaker for the PFASs with lower net negativity, interrupting the fluorous interaction to a lesser extent.

The limits of detection (LODs) for the six study PFASs with perfluoroalkyl chain lengths greater than 4 (i.e., PFHxA, PFOA, PFNA, PFDA, PFOS, and PFOPA) ranged from 0.083 to 4.962 μM. These values are comparable to the LODs for other PFAS sensors reported in the literature (Table S1). The current study focused on developing a sensing platform and understanding the working principles of the sensing instead of optimizing Citrate-Au NPs for sensitive PFAS detection. As such, there are much room for further improving the PFAS detection sensitivity. The density perfluoroalkyl receptor grafting and ζ potential of the NPs can be optimized such that the particle stability alters significantly at lower PFAS levels. The chemical structure of the perfluoroalkyl receptor, including the length of the spacer and the perfluoroalkyl carbons, is another factor that should be optimized. The sensor recipe such as the concentration of Citrate-Au NPs, and the mixing ratio between Au NP solution and target solution may also be optimized for improved sensor performance.

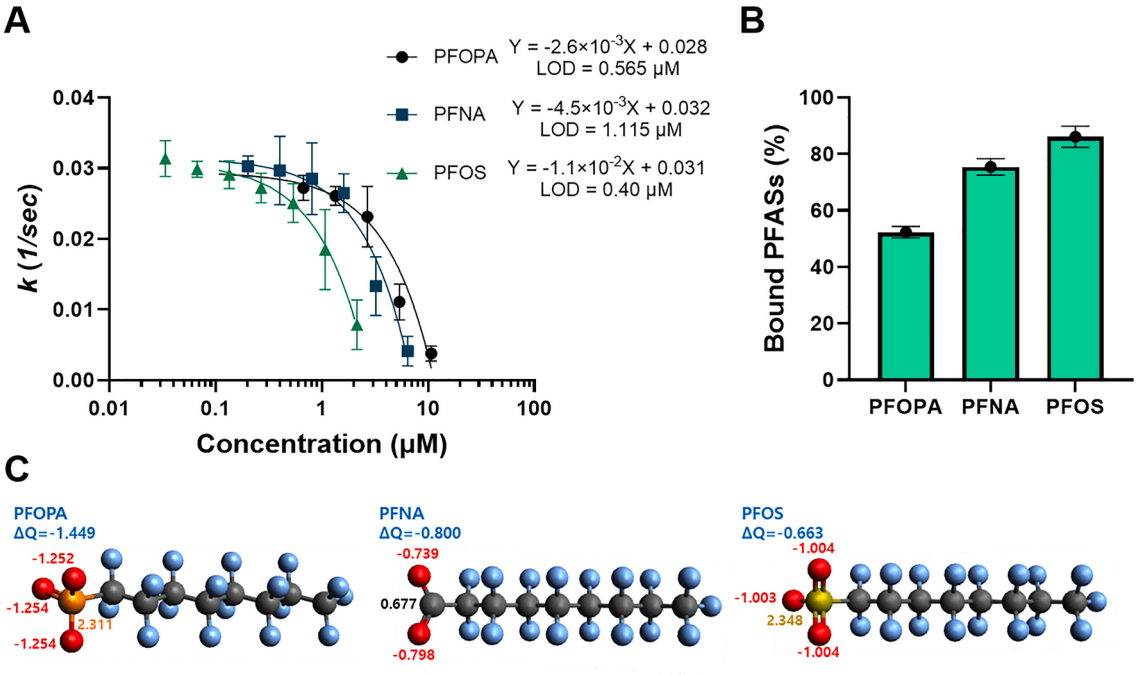

Fig. 5. (A) Response of Citrate-Au NPs sensor, (B) bound fraction of PFASs to Citrate-Au NPs, and (C) net atomic charge of functional groups for PFASs with different head groups (i.e., PFOPA, PFNA, and PFOS).

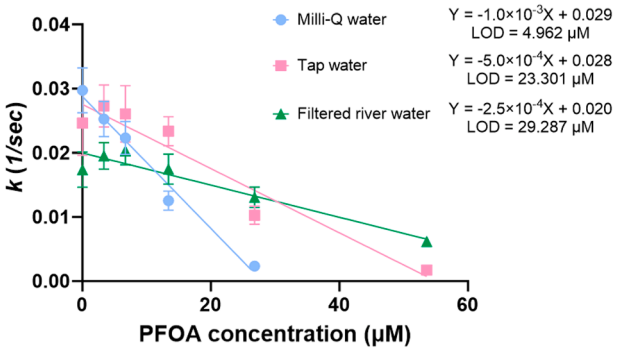

Fig. 6. PFOA calibration results for different types of water matrices: Milli-Q water, tap water, and filtered river water.

2.5. Sensor performance in various water matrix

The sensor performance in real water matrices (tap water and filtered river water) was compared with that in Milli-Q water. While the sensor responded linearly to PFOA concentration in real water matrices, the sensitivity was reduced compared to the Milli-Q water case (Fig. 6). The slope of the linear calibration curve depended on water matrix: -1.0×10^{-3} /sec/μM in Milli-Q water, -5.0×10^{-4} /sec/μM in tap water and -2.5×10^{-4} /sec/μM in filtered river water. This result shows that the Citrate-Au NPs should be calibrated using the standard solutions that possess chemical constituents close to the sample for accurate PFASs quantification.

Testing the sensor using salt-, dissolved organic matter (DOM)-, or acid/base-added Milli-Q water as target solutions identified potential contributors to the sensor signal change in real water samples. At NaCl concentration of ≥50 mM and $MgCl_2$ concentrations of ≥0.5 mM, aggregation of Au NPs occurred very rapidly, showing low A_{blue}/A_{red} value from the beginning of the spectrum measurement (Figs. S6 and S7). This result suggests that electrolytes, particularly divalent cations, significantly impact the sensor signal. At a dissolved organic carbon (DOC) concentration range from 0 to 10 mg/L, the rate of spectrum shift slowed down as DOC concentration increased (Fig. S8). A plausible explanation to this phenomenon is that DOM binds to the NP surface, retarding the aggregation of Au NPs via steric stabilization (Baalousha et al., 2013; Topuz et al., 2015). Tests performed at pH 4, 7 and 10 by acid or base addition indicate that a lower pH promotes the aggregation of Citrate-Au NPs. This suggests that protons (H^+) function similarly to other cations. The potential impact of ionic and organic water constituents on aggregation of Citrate-Au NPs underscores the necessity of constructing a calibration curve using standards close to the composition of a target solution.

3. Conclusion

This study proposed a novel colorimetric sensor that detects PFASs via the rate of spectrum shift of Citrate-Au NPs capped with a perfluoroalkyl receptor. The sensor detected medium- to long-chain PFASs (PFHxA, PFOA, PFNA, PFDA, PFOS, and PFOPA) down to sub-μM or μM level with linear responses to PFASs concentrations. Use of a perfluoroalkyl receptor to attract PFASs via fluorous interaction resulted in high selectiveness toward perfluoroalkyl carbons compared to fully hydrogenated alkyl carbons. Sensitivity of the sensor depended strongly on the chain length of the perfluoroalkyl group and the head functional group, representing the dependence of fluorous interaction on the molecular structures of PFASs. Testing the sensor performance in real water matrices showed both opportunities and challenges. The sensor worked reasonably well in tap water and surface water; however, calibration using the corresponding water matrix was necessary because the sensor response was significantly affected by DOM, divalent cations, and pH. With optimization of the NP synthesis procedure, structure of the receptor, and sensor recipe, we believe the PFASs sensing platform employed in this study can be substantially improved to allow highly sensitive and selective analysis of PFASs in water.

4. Materials and methods

4.1. Materials

Chemicals used to synthesize the Au NPs were chloroauric acid ($HAuCl_4 \bullet XH_2O$, 99.8%, Strem chemicals), sodium citrate tribasic dehydrate (for molecular biology, ≥99%, Sigma-Aldrich), 3,3,4,4,5,5,6,6,7,7,8,8,8-tridecafluoro-1-octanethiol (97%, Sigma-Aldrich), and Milli-Q water (resistivity ≈ 18.2 MΩcm, Merck Millipore®). PFBA (99%, Alfa Aesar), PFHxA (≥97%, Sigma-Aldrich), PFOA (95%, Alfa Aesar), PFNA (97%, Alfa Aesar), PFDA (96%, Sigma-Aldrich), PFOS potassium salt (≥98.0%, Sigma-Aldrich), nonanoic acid (≥97%, Sigma-Aldrich), and PFOPA (95%, Toronto Research Chemicals) were experimented as potential target chemicals for sensing. Sodium chloride (99.5%, Daejung Co., Ltd.) was used as a salt that induced aggregation of Citrate-Au NPs. For instrumental quantification of PFASs, 2000 ng/mL of native PFASs standard solution, 50 μg/mL of PFOPA standard solution, and 2000 ng/mL of ^{13}C-labeled PFASs internal standard solution were purchased from Wellington Laboratories. The solution pH was adjusted using 1 N of HCl or 2% of NaOH solution (Daejung Co., Ltd.). Suwanee River NOM (RO isolation, International Humic Substances Society) was obtained and used to represent surface water DOM.

4.2. Citrate coated gold nanoparticles (Citrate-Au NPs) synthesis

The Citrate-Au NPs were synthesized by following the Turkevich synthesis method (Turkevich et al., 1951). Twenty milliliters of 0.5 mM aqueous $HAuCl_4$ solution was boiled in a 40 mL glass vial by a hotplate stirrer combined with a heating mantle while stirring vigorously and continuously. To the boiling $HAuCl_4$ solution, 0.1 M of sodium citrate solution was added at once, and the boiling and stirring were continued for 15 min to allow reduction of Au and formation of Au NPs. The volume of the sodium citrate solution was varied such that the terminal citrate/Au molar ratio of 0.5 – 1 mmol/mmol was achieved. After cooling down the solution to room temperature, 3,3,4,4,5,5,6,6,7,7,8,8,8-tridecafluoro-1-octanethiol was added to provide perfluoroalkyl receptors to the Au NPs formed. The amount of the perfluoroalkyl receptor added was 0.5 times that of Au in terms of moles. The solution was then incubated for 24 hours without agitation in order to form the Au-S bonding.

4.3. Sensor performance test

The standard sensor recipe of the spectrum shifting assay using Citrate-Au NPs was to combine as-prepared Citrate-Au NPs solution, a target sample (i.e., solution for PFASs analysis), and NaCl solution at a volume ratio of 3:3:1 to be 0.7 mL. The first two solutions were combined first, followed by the addition of the NaCl solution. This standard recipe was determined by a trial-and-error approach. The amount of NaCl, which was used to promote aggregation of Citrate-Au NPs, was to provide NaCl concentration of 0.043 mM in the final 0.7-mL solution. After a brief manual agitation of the combined solution, it was quickly placed in a UV/Vis spectrometer (Cary UV–Vis Multicell, Agilent Technologies, Inc.) since the aggregation of Au NPs occurred immediately after the NaCl addition. The absorbance data was collected at a range of 400 – 800 nm wavelength with 1 nm of interval, 3000 nm/min of scan rate, 0.02 sec of averaging time, and 2 nm of spectral bandwidth for 5 min. The absorbance peak of an Au NPs solution slightly varies depending on the size of Au NPs (Amendola and Meneghetti, 2009; Haiss et al., 2007; Martinez et al., 2012) and the degree of dispersion (Keene

et al., 2011; Zook et al., 2011). Therefore, different wavelengths were used when reading the absorbance at red wavelength (A_{red}) and the absorbance at blue wavelength (A_{blue}) for Citrate-Au NPs synthesized at different citrate/Au molar ratios. A procedure employed to determine wavelengths for A_{red} and A_{blue} is detailed in Text S1. Calibration curves of Citrate-Au NPs were constructed by linear fitting of the performance test results using the least squares method. The limit of detection (LOD) was determined as the three standard deviations of the blank signals.

A routine procedure to prepare a target sample for the sensor performance test was to dissolve a single PFAS solute in Milli-Q water. For investigation on interference by background compositions in natural water, 53.57 μM of PFOA was spiked in Milli-Q water containing varying concentrations of $MgCl_2$, NaCl, HCl, NaOH, or DOM. $MgCl_2$ and NaCl solutions were tested at concentrations of 0.05, 0.5, 5, 50, and 500 mM and DOM at a DOC value of 0.5, 1, 3, 5, and 10 mg/L. HCl or NaOH was added to obtain a pH value of 4, 7, or 7. Additionally, the sensor performance was evaluated using collected water samples (i.e., tap water and river water) which were spiked with PFOA at a range of concentrations. The river water was collected from the intake pipe of a water purification plant in South Korea and passed through a 0.45 μm polyethersulfone membrane filter prior to use (Jet Biofiltration Co., Ltd.). Tap water was collected from a tap in the laboratory and used without pretreatment.

4.4. Investigating binding affinity between PFASs and citrate-Au NPs

The dependence of PFASs functional group on their binding affinity to the receptor of Citrate-Au NPs was investigated. To this end, three different PFASs with identical perfluoroalkyl carbon chain length (C = 8) but with different functional groups such as carboxylic acid (PFNA), sulfonic acid (PFOS), and phosphonic acid (PFOPA) were studied. The Citrate-Au NPs solution, a solution containing one of the three PFASs, and Milli-Q water instead of NaCl were mixed at a volume ratio of 3:3:1 to mimic the sensor recipe. After a vigorous hand-mixing, the solution was filtered with an Amicon filter (3 kDa MWCO) through centrifugation at 13,000 rpm to separate unbound PFASs. The percentage of PFASs bound to Citrate-Au NPs (Bound PFASs,%) was determined as the ratio of the difference between the initial PFASs concentration and PFASs concentration after the filtration relative to the initial PFASs concentration.

4.5. Analytical methods

The hydrodynamic particle sizes of the synthesized Au NPs were measured with DLS (Zetasizer Nano ZS, Malvern Panalytical) at 25 °C with 90° measurement angle. The refractive index (RI) and the absorption value of Au NPs was set as 0.2 and 3.320, respectively, and the viscosity and RI of solution (i.e., water) as 0.8872 mPa•s and 1.330, respectively, following the Malvern software. The DLS measurement result was cross-validated using an image obtained using TEM (JEM 1010, JEOL Ltd.), which was operated at an accelerating voltage of 80 kV. The size of Au NPs in the TEM image was analyzed with an image analysis tool, image J.

The amount of Au NPs available in solution for sensing was determined as follows. One milliliter of Au NPs solution was retrieved from a synthesized batch and placed in a 15-mL conical tube. All the Au NPs in the solution were converted to Au ions by adding 2 mL of aqua regia and 1 mL of hydrogen peroxide. The digested solution was diluted with an acid solution containing 0.5% of HCl and 1% of HNO_3 prior to analysis. Au was analyzed using inductively coupled plasma optical emission spectrometry (ICP-MS 7800, Agilent Technologies, Inc.) equipped with a MicroMist nebulizer and a nickel sampler cone. The operation conditions were optimized with automatic tuning using Agilent ICP-MS tuning solution before the analysis. The integration time/mass was set as 0.3. The Au concentration determined by this procedure allowed calculation of the yield fraction of Au NPs ($M_{Au\ NPs}/M_{Au0}$).

The concentrations of PFOS, PFNA, and PFOPA was determined with liquid chromatography (1290 infinity II, Agilent Technologies, Inc.) coupled to a triple quadrupole mass spectrometer (6470 LC-MS/MS, Agilent Technologies, Inc.). Analytes were separated using a ZORBAX RRHD eclipse plus C18 (95 Å, 2.1 × 100 mm, 1.8 μm, Agilent Technologies, Inc.) column and an InfinityLab PFC delay column (4.6 × 30 mm, Agilent Technologies, Inc.). Samples were injected at an amount of 5 μL and detected using the dynamic multiple reaction monitoring method. The gas temperature and flow rate were 350 °C and 4 L/min, respectively. Eluents were composed of 20 mM of ammonium acetate in Milli-Q water and methanol, which flowed at 0.4 L/min. The eluent gradient program and mass spectral parameters are given in Tables S2 and S3. The MS was run in negative ionization mode with the following details: nebulizer pressure of 15 psi, sheath gas temperature of 350 °C, flowrate of 12 L/min, and capillary voltage of 2500 V (pos.) and 2500 V (neg.).

Total organic carbon (TOC) content of the river water was analyzed with the non-purgeable organic carbon method using a TOC analyzer (ASI-V, Shimadzu). Electrical conductivity and pH were measured with Orion Star™ A325 (Thermo Scientific). ζ potential was measured with Zetasizer Nano ZS (Malvern Panalytical).

4.6. Computational determination of net atomic charge of PFASs

The natural population analysis (NPA) was conducted to calculate the net atomic charges of PFOS, PFNA, and PFOPA using a DFT simulation program. The DFT simulation was performed with ORCA 5.03 software by following the method described in Park et al. (Park et al., 2020). The geometries of PFASs were drawn and optimized with MMFF94 force fields using Avogadro software to generate input files for DFT analysis. Geometry optimization of molecules was performed before simulation using B3LYP functional. For basis set and auxiliary basis set, def2-TZPP and def2-TZPP/C were adopted, respectively. SCF convergence tolerance was set to be VeryTightSCF. The effect of water was analyzed with conductor-like polarizable continuum model. Then, from the DFT simulation result, the NPA result was obtained with JANPA software, an open source program.

CRediT authorship contribution statement

Jihyeun Jung: Writing – original draft, Visualization, Validation, Methodology, Investigation, Formal analysis, Data curation. **Junyoung Park:** Software, Investigation, Data curation. **Jong Kwon Choe:** Writing – review & editing, Supervision, Methodology, Conceptualization. **Yongju Choi:** Writing – review & editing, Supervision, Resources, Project administration, Methodology, Funding acquisition, Conceptualization.

Declaration of competing interest

The authors declare that they have no known competing financial interests or personal relationships that could have appeared to influence the work reported in this paper.

Data availability

Data will be made available on request

Acknowledgments

This work was supported by the National Research Foundation of Korea (NRF) grant funded by the Korea government (MSIT) (no. NRF-2021R1A4A1026364) and the Korea Environment Industry & Technology Institute (KEITI) through “Project for developing innovative drinking water and wastewater technologies” (2019002710002), funded by

the Korea Ministry of Environment (MOE). The authors would like to thank the Institute of Engineering Research at Seoul National University for their technical assistance.

Supplementary materials

Supplementary material associated with this article can be found, in the online version, at doi:10.1016/j.wroa.2024.100239.

References

Aldewachi, H., Chalati, T., Woodroofe, M.N., Bricklebank, N., Sharrack, B., Gardiner, P., 2018. Gold nanoparticle-based colorimetric biosensors. Nanoscale 10, 18–33. https://doi.org/10.1039/c7nr06367a.

Amendola, V., Meneghetti, M., 2009. Size evaluation of gold nanoparticles by UV-vis spectroscopy. J. Phys. Chem. C 113, 4277–4285. https://doi.org/10.1021/jp8082425.

Amin, A.M., Sobhani, Z., Chadalavada, S., Naidu, R., Fang, C., 2020. Smartphone-based /fluoro-SPE for selective detection of PFAS at ppb level. Environ. Technol. Innov. 18, 100778 https://doi.org/10.1016/J.ETI.2020.100778.

Baalousha, M., Nur, Y., Römer, I., Tejamaya, M., Lead, J.R., 2013. Effect of monovalent and divalent cations, anions and fulvic acid on aggregation of citrate-coated silver nanoparticles. Sci. Total Environ. 454–455, 119–131. https://doi.org/10.1016/J.SCITOTENV.2013.02.093.

Barisik, M., Atalay, S., Beskok, A., Qian, S., 2014. Size dependent surface charge properties of silica nanoparticles. J. Phys. Chem. C 118, 1836–1842. https://doi.org/10.1021/jp410536n.

Bigdeli, A., Ghasemi, F., Golmohammadi, H., Abbasi-Moayed, S., Amin, M., Nejad, F., Fahimi-Kashani, N., Jafarinejad, S., Shahrajabian, M., Reza Hormozi-Nezhad, M., 2017. Nanoparticle-based optical sensor arrays. Nanoscale 9, 16546. https://doi.org/10.1039/c7nr03311g.

Chen, H., Zhou, K., Zhao, G., 2018. Gold nanoparticles: from synthesis, properties to their potential application as colorimetric sensors in food safety screening. Trends Food Sci. Technol. 78, 83–94. https://doi.org/10.1016/j.tifs.2018.05.027.

Dalvi, V.H., Rossky, P.J., 2010. Molecular origins of fluorocarbon hydrophobicity. Proc. Natl. Acad. Sci. U.S.A. 107, 13603–13607. https://doi.org/10.1073/PNAS.0915169107.

Du, Z., Deng, S., Zhang, S., Wang, B., Huang, J., Wang, Y., Yu, G., Xing, B., 2016. Selective and high sorption of perfluorooctanesulfonate and perfluorooctanoate by fluorinated alkyl chain modified montmorillonite. J. Phys. Chem. C 120, 16782–16790. https://doi.org/10.1021/acs.jpcc.6b04757.

Ellis, D.A., Denkenberger, K.A., Burrow, T.E., Mabury, S.A., 2004. The Use of 19F NMR to interpret the structural properties of perfluorocarboxylate acids: a possible correlation with their environmental disposition. J. Phys. Chem. A 108, 10099–10106. https://doi.org/10.1021/jp049372a.

Fang, C., Dharmarajan, R., Megharaj, M., Naidu, R., 2017. Gold nanoparticle-based optical sensors for selected anionic contaminants. Trend. Anal. Chem. 86, 143–154. https://doi.org/10.1016/j.trac.2016.10.008.

Fenton, S.E., Ducatman, A., Boobis, A., Dewitt, J.C., Lau, C., Ng, C., Smith, J.S., Roberts, S.M., 2021. Per-and polyfluoroalkyl substance toxicity and human health review: current state of knowledge and strategies for informing future research. Environ. Toxicol. Chem. 40, 606–630. https://doi.org/10.1002/etc.4890.

Garnett, J., Halsall, C., Thomas, M., Crabeck, O., France, J., Joerss, H., Ebinghaus, R., Kaiser, J., Leeson, A., Wynn, P.M., 2021. Investigating the uptake and fate of poly- and perfluoroalkylated substances (PFAS) in sea ice using an experimental sea ice chamber. Environ. Sci. Technol 55, 9601–9608. https://doi.org/10.1021/acs.est.1c01645.

Guo, T.-Y., Li, H.-W., Zhang, C.-X., Wu, Y., 2023. The colorimetry and smartphone determination of perfluorooctane sulfonate based on cytidine 5'-monophosphate-capped gold nanoclusters with peroxidase-like activity. Analyst 148, 3931–3937. https://doi.org/10.1039/d3an00763d.

Haiss, W., Thanh, N.T.K., Aveyard, J., Fernig, D.G., 2007. Determination of size and concentration of gold nanoparticles from UV−Vis spectra. Anal. Chem. 79, 4215–4221. https://doi.org/10.1021/ac0702084.

Harris, M.H., Rifas-Shiman, S.L., Calafat, A.M., Ye, X., Mora, A.M., Webster, T.F., Oken, E., Sagiv, S.K., 2017. Predictors of per-and polyfluoroalkyl substance (PFAS) plasma concentrations in 6−10 year old American children. In: Environ. Sci. Technol., 51, pp. 5193–5204. https://doi.org/10.1021/acs.est.6b05811.

Ji, X., Song, X., Li, J., Bai, Y., Yang, W., Peng, X., 2007. Size control of gold nanocrystals in citrate reduction: the third role of citrate. In: J. Am. Chem. Soc., 129, pp. 13939–13948. https://doi.org/10.1021/ja074447k.

Jiang, X., Wang, W., Yu, G., Deng, S., 2021. Contribution of nanobubbles for PFAS adsorption on graphene and OH-and NH 2-functionalized graphene: comparing simulations with experimental results. Cite This Environ. Sci. Technol. 55, 13254–13263. https://doi.org/10.1021/acs.est.1c03022.

Jing, P., Rodgers, P.J., Amemiya, S., 2009. High lipophilicity of perfluoroalkyl carboxylate and sulfonate: implications for their membrane permeability. J. Am. Chem. Soc. 131, 2290–2296. https://doi.org/10.1021/ja807961s.

Johnson, J.K., Hoffman, C.M., Smith, D.A., Xia, Z., 2019. Advanced filtration membranes for the removal of perfluoroalkyl species from water. ACS Omega 49, 22. https://doi.org/10.1021/acsomega.9b00314.

Keene, Athena M, Tyner, K.M., Keene, A.M., Tyner, Á.K.M., 2011. Analytical characterization of gold nanoparticle primary particles, aggregates, agglomerates, and agglomerated aggregates. J. Nanopart. Res. 13, 3465–3481. https://doi.org/10.1007/s11051-011-0268-4.

Kiss, L.E., Kövesdi, I., Rábai, J, 2001. An improved design of fluorophilic molecules: prediction of the ln P fuorous partition coeffcient, fluorophilicity, using 3D QSAR descriptors and neural networks. J. Fluor. Chem. 108, 95–109. https://doi.org/10.1016/S0022-1139(01)00342-6.

Kobayashi, M., Juillerat, F., Galletto, P., Bowen, P., Borkovec, M., 2005. Aggregation and charging of colloidal silica particles: Effect of particle size. In: Langmuir, 21, pp. 5761–5769. https://doi.org/10.1021/la046829z.

Krafft, M.P., Riess, J.G., 2009. Chemistry, physical chemistry, and uses of molecular fluorocarbon-hydrocarbon diblocks, triblocks, and related compoundssunique "apolar" components for self-assembled colloid and interface engineering. Chem. Rev. 109, 1714–1792. https://doi.org/10.1021/cr800260k.

Lambros, M., Tran, T., Fei, Q., Nicolaou, M., 2022. Citric acid: a multifunctional pharmaceutical excipient. Pharmaceutics 14, 972. https://doi.org/10.3390/pharmaceutics14050972.

Lee, J.H., Wang, Z., Liu, J., Lu, Y., 2008. Highly sensitive and selective colorimetric sensors for uranyl (UO_2^{2+}): development and comparison of labeled and label-free DNAzyme-gold nanoparticle systems. J. Am. Chem. Soc. 130, 14217. https://doi.org/10.1021/ja803607z. –14217.

Lee, J.W., Choi, S.-R., Heo, J.H., 2021. Simultaneous stabilization and functionalization of gold nanoparticles via biomolecule conjugation: progress and perspectives. ACS Appl. Mater. Interface. 13, 42311–42328. https://doi.org/10.1021/acsami.1c10436.

Liu, J., Du, J., Su, Y., Zhao, H., 2019. A facile solvothermal synthesis of 3D magnetic MoS_2/Fe_3O_4 nanocomposites with enhanced peroxidase-mimicking activity and colorimetric detection of perfluorooctane sulfonate. Microchem. J. 149, 104019 https://doi.org/10.1016/J.MICROC.2019.104019.

Martinez, J.C., Chequer, N.A., Gonzalez, J.L., Cordova, T., 2012. Alternative metodology for gold nanoparticles characterization diameter using PCA technique and UV-VIS spectrophotometry. Nanosci. Nanotechnol. 2, 184–189. https://doi.org/10.5923/j.nn.20120206.06.

Menger, R.F., Beck, J.J., Borch, T., Henry, C.S., 2022. Colorimetric paper-based analytical device for perfluorooctanesulfonate detection. ACS ES&T Water 2, 565–572. https://doi.org/10.1021/acsestwater.1c00356.

Menger, R.F., Funk, E., Henry, C.S., Borch, T., 2021. Sensors for detecting per- and polyfluoroalkyl substances (PFAS): a critical review of development challenges, current sensors, and commercialization obstacles. Chem. Eng. J. 417 https://doi.org/10.1016/J.CEJ.2021.129133.

Ojea-Jiménez, I., Romero, F.M., Bastú, N.G., Puntes, V., 2010. Small gold nanoparticles synthesized with sodium citrate and heavy water: insights into the reaction mechanism. J. Phys. Chem. C 114, 1800–1804. https://doi.org/10.1021/jp9091305.

Omorodion, H., Twamley, B., Platts, J.A., Baker, R.J., 2015. Further evidence on the importance of fluorous−fluorous interactions in supramolecular chemistry: A combined structural and computational study. In: Cryst. Growth Des., 15, pp. 2835–2841. https://doi.org/10.1021/acs.cgd.5b00254.

Osei-Prempeh, G., Lehmler, H.J., Rankin, S.E., Knutson, B.L., 2008. Synthesis of fluoro-functionalized mesoporous silica and application to fluorophilic separations. Ind. Eng. Chem. Res. 47, 530–538. https://doi.org/10.1021/ie070538e.

Park, M., Daniels, K.D., Wu, S., Ziska, A.D., Snyder, S.A., 2020. Magnetic ion-exchange (MIEX) resin for perfluorinated alkylsubstance (PFAS) removal in groundwater: roles of atomic charges for adsorption. Water Res 181, 115897. https://doi.org/10.1016/J.WATRES.2020.115897.

Pétré, M.A., Genereux, D.P., Koropeckyj-Cox, L., Knappe, D.R.U., Duboscq, S., Gilmore, T.E., Hopkins, Z.R., 2021. Per-and polyfluoroalkyl substance (PFAS) transport from groundwater to streams near a PFAS manufacturing facility in North Carolina, USA. Environ. Sci. Technol. 55, 5848–5856. https://doi.org/10.1021/acs.est.0c07978.

Piella, J., Bastús, N.G., Puntes, V., 2016. Size-controlled synthesis of sub-10-nanometer citrate-stabilized gold nanoparticles and related optical properties. Chem. Mater. 28, 1066–1075. https://doi.org/10.1021/acs.chemmater.5b04406.

Pochapski, D.J., Carvalho dos Santos, C., Leite, G.W., Pulcinelli, S.H., Santilli, C.V., 2021. Zeta potential and colloidal stability predictions for inorganic nanoparticle dispersions: effects of experimental conditions and electrokinetic models on the interpretation of results. Langmuir 37, 13379–13389. https://doi.org/10.1021/acs.langmuir.1c02056.

Pollice, R., Chen, P., 2019. Origin of the immiscibility of alkanes and perfluoroalkanes. J. Am. Chem. Soc. 141, 3489–3506. https://doi.org/10.1021/jacs.8b10745.

Polte, J., Ahner, T.T., Delissen, F., Sokolov, S., Emmerling, F., Thü, A.F., Kraehnert, R., 2010. Mechanism of gold nanoparticle formation in the classical citrate synthesis method derived from coupled in situ XANES and SAXS evaluation. J. Am. Chem. Soc. 132, 1296–1301. https://doi.org/10.1021/ja906506j.

Robalo, J.R., Mendes de Oliveira, D., Ben-Amotz, D., Villa Verde, A., 2021. Influence of methylene fluorination and chain length on the hydration shell structure and thermodynamics of linear diols. J. Phys. Chem. B 125, 2023. https://doi.org/10.1021/acs.jpcb.1c08601.

Ryu, H., Li, B., Guise, S.De, McCutcheon, J., Lei, Y., 2021. Recent progress in the detection of emerging contaminants PFASs. J. Hazard. Mater. 408, 124437 https://doi.org/10.1016/J.JHAZMAT.2020.124437.

Santiago, A.R., Yin, S., Elbert, J., Lee, J., Shukla, D., Su, X., 2023. Imparting selective fluorophilic interactions in redox copolymers for the electrochemically mediated capture of short-chain perfluoroalkyl substances. J. Am. Chem. Soc. 145, 95089519 https://doi.org/10.1021/jacs.2c10963.

Taylor, C.M., Breadmore, M.C., Kilah, N.L., 2023. Colorimetric determination of perfluorocarboxylic acids using porphyrin hosts and mobile phone photographs. Sens. Diagn 2, 676–696. https://doi.org/10.1039/d3sd00035d.

Taylor, C.M., Ellingsen, T.A., Breadmore, M.C., Kilah, N.L., 2021. Porphyrin-based colorimetric sensing of perfluorooctanoic acid as proof of concept for perfluoroalkyl substance detection. Chem. Commun 57, 11649–11652. https://doi.org/10.1039/d1cc04903h.

Topuz, E., Traber, J., Sigg, L., Talinli, I., 2015. Agglomeration of Ag and TiO_2 nanoparticles in surface and wastewater: role of calcium ions and of organic carbon fractions. Environ. Pollut. 204, 313–323. https://doi.org/10.1016/J.ENVPOL.2015.05.034.

Turkevich, J., Stevenson, P.C., Hillier, J., 1951. A study of the nucleation and growth processes in the synthesis of colloidal gold. Discuss. Faraday Soc. 11, 55–75.

Umapathi, R., Park, B., Sonwal, S., Rani, G.M., Cho, Y., Huh, Y.S., 2022. Advances in optical-sensing strategies for the on-site detection of pesticides in agricultural foods. Trend. Food Sci. Technol. 119, 69–89. https://doi.org/10.1016/J.TIFS.2021.11.018.

Wang, Y., Darling, S.B., Chen, J., 2021. Selectivity of per-and polyfluoroalkyl substance sensors and sorbents in water. ACS Appl. Mater. Interface. 13, 60789–60814. https://doi.org/10.1021/acsami.1c16517.

Wei, X., Popov, A., Hernandez, R., 2022. Electric potential of citrate-capped gold nanoparticles is affected by poly(allylamine hydrochloride) and salt concentration. ACS Appl. Mater. & Interfaces 14, 12538–12550. https://doi.org/10.1021/acsami.1c24526.

Zabetakis, K., Ghann, W.E., Kumar, S., Daniel, M.C., 2012. Effect of high gold salt concentrations on the size and polydispersity of gold nanoparticles prepared by an extended Turkevich-Frens method. In: Gold Bulletin, 45, pp. 203–211. https://doi.org/10.1007/s13404-012-0069-2.

Zheng, G., Schreder, E., Dempsey, J.C., Uding, N., Chu, V., Andres, G., Sathyanarayana, S., Salamova, A., 2021. Per-and polyfluoroalkyl substances (PFAS) in breast milk: concerning trends for current-use PFAS. Environ. Sci. Technol 55. https://doi.org/10.1021/acs.est.0c06978.

Zook, J.M., Rastogi, V., MacCuspie, R., Keene, A.M., Fagan, J., 2011. Measuring agglomerate size distribution and dependence of localized surface plasmon resonance absorbance on gold nanoparticle agglomerate size using analytical ultracentrifugation. ACS Nano 5, 8070–8079. https://doi.org/10.1021/nn202645b.